Cement and Concrete Composites 139 (2023) 105058

Contents lists available at ScienceDirect

Cement and Concrete Composites

journal homepage: www.elsevier.com/locate/cemconcomp

A methodology to assess the evolution of mechanical performance of UHPC as affected by autogenous healing under sustained loadings and aggressive exposure conditions

Marco Davolio [a,*], Salam Al-Obaidi [a,b], Maria Ylenia Altomare [a], Francesco Lo Monte [a], Liberato Ferrara [a]

[a] Department of Civil and Environmental Engineering, Politecnico di Milano, Milan, Italy
[b] Roads and Transportations Engineering Department, University of Al-Qadisiyah, Diwaniyah, Iraq

A B S T R A C T

This study investigates the evolution of the performance of an Ultra-High Performance Concrete (UHPC) under simultaneous action of sustained loading and aggressive environmental exposure. UHPC mixes were investigated containing different functionalizing micro- and nano-scale components to promote autogenous self-healing. In order to assess the healing capabilities in the different multi-action scenarios and the evolution of the mechanical response of the material over time, a tailored methodology was implemented, including non-destructive and destructive tests performed all along the scheduled exposure/healing times up to 12 months. In particular, an innovative set-up was designed to reproduce on the specimens the sustained flexural loading conditions a structure undergoes during its service life; the load was applied simultaneously with each of the three selected different exposures, to simulate the chloride and sulphate aggressive environments, besides a reference one. Multiple indices were defined to quantify the self-healing efficiency, which were further calibrated against experimental microscope crack observation as well as cross correlated with each other, as a further proof of the reliability of the proposed methodology. The results confirmed the material durability, especially in the cracked state, through its capacity of sealing the cracks and restoring original properties in short periods and preserving its load bearing capacity, thus providing solid argument for UHPC as the ideal candidate material for highly durable and sustainable structural applications in aggressive scenarios.

1. Introduction

Reinforced concrete structures, including marine structures, transportation infrastructures and facilities for chemical industries, are severely susceptible to degradation and deterioration due to the extremely aggressive conditions applied on the structures throughout their service life. Such deterioration does not only affect the structure service life, but also increases the operational cost all along the life cycle due to the need for multiple repairs and retrofitting [1–3]. As a matter of fact, the corrective and preventive maintenance cost of the chemical plants can reach 30% of the annual operating budget [4]. Nonetheless, repairing and reconstructing these structures emphasizes the problem of materials consumption, worsening the related environmental impact. Therefore, it is essential to use durable materials to ensure a sustainable design for the construction of these structures. Owing to its properties, Ultra-High (Fibre Reinforced) Performance Concrete (UHPFRC/UHPC) can mitigate the main inadequacies of ordinary reinforced concrete [5–7]. Hence, it is considered one of the most attractive alternatives for industrial and offshore construction materials. UHPC features on the one hand a remarkable compressive strength [8] and reliable tensile resistance [9], owing to its low binder-to-cement ratio, high density, and well-distributed micro-steel fibres, thus allowing to significantly reduce the size of element section [10,11]. Moreover, relevant flexural strength is achieved [12,13], possibly reducing or eliminating traditional reinforcement; therefore, the section of the UHPC element can be considered entirely reactive, both under compression and tension. On the other hand, thin elements are susceptible to significant deformations and, consequently, cracks on the tensile face should be expected. The short, dispersed steel fibres are engaged in bridging the cracks as soon as they occur, controlling crack width and hence further limiting the penetration and ingress of aggressive substances [14]. Fibres content of UHPC does not only provide damage control by means of crack bridging, but also promotes the development of a multiple cracking regime, since the energy required to form new cracks is lower than the work needed to pull-out the fibres at the formed crack and experience the localisation [15–17]. Subsequently, the mechanical response of the material shows a strain-hardening behaviour up to the localisation of one major unstable crack; hence, UHPC tensile performance significantly improves in the

* Corresponding author.
E-mail address: marco.davolio@polimi.it (M. Davolio).

https://doi.org/10.1016/j.cemconcomp.2023.105058
Received 30 December 2022; Received in revised form 15 March 2023; Accepted 29 March 2023
Available online 30 March 2023

cracked state, fostering the design of thin elements to exploit the strain-hardening response of the material [18]. Therefore, it is crucial to prevent degradation and to protect steel fibres, strongly susceptible to corrosion phenomena [19]. Moreover, UHPC is characterised by a significant autogenous self-healing capacity. Self-healing is triggered by the formation of cracks on the concrete matrix, since UHPC, owing to its low w/b ratio, is rich in un-hydrated cement particles that start reacting with water. Also, the void created between crack surfaces accommodates precipitates due to chemical processes or inherently present in the environmental exposure. The sealing of the cracks is crucial to protect steel fibres activated during the cracking phase from corrosion and, thus, its effectiveness must be investigated [20]. Furthermore, healing processes are not instantaneous and their evolution over time plays a fundamental role in preserving the tensile resistance of UHPC, which could deteriorate when the material is exposed to aggressive environments.

Even though the application of UHPC seems advantageous exactly in structures whose durability requirements are particularly essential, the market response is lagging behind due to the long term required for the development of internationally recognized material standards and design codes [21]. Currently, to ensure that a concrete structure meets the durability requirements, two different methods are available in the design codes: prescriptive (i.e., deemed to satisfy) and performance-based. Each approach has its own unique weaknesses and strengths [22,23]. Whenever a new category of advanced cement-based materials is going to be employed, the performance-based approach is more pertinent, and needs to be tailored starting from laboratory investigations and theoretical modelling of the material and elements behaviour. The information gathered allows the design of real structures which have then to be validated through continuous monitoring and observation.

Durability design of UHPC [24,25], as previously stated, is not limited to passive prescriptions; instead, self-healing mechanisms must be considered, since they preserve the tensile performance of the material in cracked state. Therefore, the mechanical response of the material over time should be determined under real structural conditions, both at macro- and mesoscale levels, including self-healing contribution as well as structural and environmental actions.

Only few studies on UHPC long term durability with simultaneous presence of mechanical and chemical loads are currently available. Graybeal [26] investigated the response of a rectangular UHPC beam with a cross section of 152 × 381 mm^2 and a span length of 5 m, reinforced with two Ø12 mm steel rebars with 35 mm cover. The beam went under 500.000 cycles of four-point bending flexural loading, with the tensile face was simultaneously exposed to a chloride impregnated sponge, positioned at the tensile face to transport the 15% NaCl solution through the cracks formed by the bending action. No visible deterioration occurred, and the penetration of the chlorides was limited to 3 mm through the tensile face. The mechanical response, measured by means of direct tensile tests on prisms extracted from the tensile face of the beam near the flexural failure location, did not exhibit any degradation, and the steel fibres did not show any visible signs of tensile failure or section loss. Moffatt et al. [27] studied 152 × 152 × 533 mm^3 reinforced concrete prisms made of different materials, reactive powder concrete (RPC), very-high strength concrete (VHSC), and UHPC. The specimens were exposed to sustained loading and environmental exposure in the Gulf of Maine (US), in mid tide level (3.52% salinity) and experienced from 100 to 160 freeze-thaw cycles per year. Even after 12 years no significant deterioration was detected on UHPC with reference to mechanical performance, and similar results were observed for VHSC and RPC after 5–21 years. In terms of chloride ingress, the long-term exposure did not affect the penetration depth, as most of the phenomenon developed during the first 5 years; owing to their reduced permeability, the UHPC specimens experienced a significant resistance to the chloride penetration, even compared with the HPC specimens. The works herein presented proved the excellent performance of the material, but self-healing mechanisms were not considered, as well as a reference condition without aggressive agents.

UHPC autogenous self-healing capability was at first analysed separately addressing durability or mechanical recovery. The durability performance was evaluated by means of permeability tests, resonant frequency, ultrasonic measurements, and resistance against corrosion [28–33]. For the mechanical recovery, studies were conducted on compressive strength, flexural performance, tensile performance, and stiffness recovery [28–32,34,35]. Beglarigale et al. [36] determined the self-healing capacity of a UHPC mix through different techniques referred to durability, but only considering compressive strength in terms of mechanical recovery.

Özbay et al. [37] studied 360 × 50 × 75 mm^3 prisms, pre-cracked with reference to the mid-span deflection (2.5 mm), and then exposed inside the ageing chamber to either air or water for up to 90 days; a sustained load device was applied to half of the specimens, keeping the prisms at 60% of the flexural ultimate load. Water played a key role in the mechanical recovery, promoting the formation of healing products, thus enhancing the flexural stiffness and the flexural deflection capacity. On the other hand, the sustained mechanical loading partially affected the self-healing effects, since, according to the authors, the cracks formed during the pre-cracking phase widened instead of closing. Parant et al. [38] presented a broad experimental campaign on self-healing of a UHPC, pre-cracking thin slabs by fatigue under service loading and maintaining the bending condition applied. In the meanwhile, the slabs underwent wetting-drying cycles in a chloride solution (5% NaCl). Even under sustained loading and environmental aggression, the UHPC investigated showed absence of corrosion and a quasi-total recovery of the initial stiffness. Various other studies addressed the self-healing capacity of UHPC with load constantly applied, but only with reference to the permeability of the material [39–41].

UHPC showed remarkable potential for the introduction of a new durability assessment-based design approach concept for structural design, for which the material not only has to preserve steel reinforcement from aggressive agents, but also must play an active role guaranteeing a constant mechanical performance over time. Moreover, since the main innovative feature of UHPC is its tensile resistance, a study on the long-term durability should tackle the evolution of the latter over time in real service life conditions, including loads applied to the structural element, possible aggressive exposures affecting the material, and self-healing effects on the mechanical recovery, as herein proposed.

2. Materials

The H2020 ReSHEALience project has developed the concept of Ultra High Durability Concrete (UHDC) [42], defined as a "strain-hardening (fibre reinforced) cementitious material with functionalizing micro- and nano-scale constituents (alumina nanofibers, cellulose nanofibers/crystals, crystalline admixtures), especially added to obtain a high durability in the cracked state".

To achieve the intended behaviour, a specific mix design has been developed, introducing crystalline admixture to promote the autogenous self-healing capacity [43,44], and nano-constituents [45], whose contribution is herein investigated.

Table 1 describes the composition of the different UHDC mixes, distinguishing three types of batches: with alumina nano-fibres (CA + ANF), with cellulose nanocrystals (CA + CNC), and without nano materials, assumed as a reference (CA-REF). A Portland cement (CEM I 52.5 R) combined with slag was used, with a water-to-binder ratio of 0.18. The volume ratio of steel fibres is 1.5%. To ensure a proper dispersion of the components of the mix, and to cope with the viscosity of the sonicated suspension, the specific mixing protocol proposed by Cuenca et al. [44] and reported in Table 2 was followed.

Table 1
UHDC mix design, components, and proportions.

Constituents [kg/m^3]	CA-REF	CA + ANF	CA + CNC
CEM I 52.5 R	600	600	600
Slag	500	500	500
Water	200	200	200
Steel fibres Azichem Readymesh 200®	120	120	120
Sand (Ø ≤ 2 mm)	982	982	982
Superplasticiser MasterGlenium ACE 300®	33	33	33
Crystalline admixture Penetron Admix®	4.8	4.8	4.8
Alumina nano-fibres* NAFEN®	–	0.25	–
Cellulose nano-crystals* Navitas®	–	–	0.15

*% by weight of cement.

Table 2
Mixing protocol from Cuenca et al. [44].

Operation	Time [min]
Dry mixing of cement, slag, CA and sand	0–2
Addition of water and superplasticiser	2–3
Addition of ANF/CNC suspension*	3–4
High speed mixing	4–19
Addition of steel fibres	19–20
High speed mixing	20–23

*in CA + ANF and CA + CNC mixes respectively.

3. Experimental methodology

The implementation of UHDC materials into real scale structures requires the same knowledge presently available on ORC to be garnered with specific regards to long term performance prediction. As a consequence, a new methodology to assess the performance evolution over time of the UHDC materials is herein proposed.

3.1. Specimen production

In the ReSHEALience project framework, real structures made of UHDC materials have been designed and built to prove the concept of the newly adopted materials [46]. One of the pilot structures is a basin for the collection of geothermal water in a geothermal power plant located in Chiusdino (Siena, Italy), owned and operated by Enel Green Power (EGP), partner of the ReSHEALience project. The basin is divided into three different compartments, the first being made of 100 mm thick ordinary reinforced concrete walls, while the others are entirely built with UHDC. The second compartment consists of 60 mm thick UHDC walls, whereas a different structural concept has been adopted for the third, made of 30 mm thick precast UHDC slabs supported by 200 × 200 mm^2 UHDC columns. A more detailed description of the pilot can be found in Refs. [11,24].

The UHDC specimens used in this study were casted on site during the construction of the pilot structure in February 2020. Taking into consideration the sensitivity of highly flowable cement-based materials to the casting method (i.e., direction of the casting, shape of the mould, handling and pouring of the material) [47,48], the experimental campaign aimed at including any possible influence that might occur during the process. Six different slabs with dimensions of 165 × 150 mm^2 and nominal thickness of 30 mm were casted on site, two per batch. Before cutting the panels into the laboratory specimen dimensions, steel fibres survey by means of non-destructive measurements was carried out with a specific magnetic sensor [49–51], consisting of two probes spaced at 160 mm which create a magnetic field and a main body where the inductance is recorded; since the inductance is affected by the steel fibre content and orientation, the variations measured allow to draw a qualitative map of the fibre dispersion. After the magnetic survey, each panel was cut into 500 × 100 × 30 mm^3 thin beams, whose position and relative fibre content could be traced according to the inductance map. A total of 216 beams was used for the experimental campaign.

3.2. Experimental programme

The methodology herein proposed was developed over different steps, including non-destructive and destructive tests, the latter being either a four-point bending flexural test or a direct tensile test, performed at the end of the process. The scheme in Fig. 1 highlights the role of both the nano-additive contribution and the exposure scenario as experimental variables. For each possible condition, two coupled beams were tested, as will be later clarified. While for the first three months of exposure the tests were performed every month, the time step was then extended to three months, ensuring three nominally identical results.

The general layout of the tests performed is shown in Fig. 2. Three different stages can be distinguished: (i) uncracked specimen, (ii) pre-cracked specimen, and (iii) cured/healed specimen (i.e., after exposure). At each stage non-destructive tests were performed, namely ultrasonic pulses velocity (UPV) and natural frequency of vibration (NFV) tests, and at stage (iii) the failure tests were performed. The crack width was also measured at stages (ii) and (iii).

3.3. Steel fibres survey

The non-destructive magnetic survey was performed with a specific sensor to evaluate the steel content inside the UHDC panels. The slabs were marked with a 160 × 160 mm^2 grid, and inside each cell four measures were taken, rotating the sensor each time by 45°, since the sensor readings are affected by the orientation of the fibres (Fig. 3). No relevant differences were recorded among the single cells' values, allowing the average value to be taken as reference. Moreover, since the variability among the orientations was less than 1%, all the specimens were considered nominally identical, regardless of the cutting direction. The inductance results were calibrated on a panel with a known fibre content of 120 kg/m^3, as prescribed by the mix design of the UHDC. Therefore, it was possible to correlate the measures taken with a qualitative estimate of the fibre content following the methodology explained in Ref. [51].

3.4. Non-destructive tests

Two different non-destructive tests were executed to evaluate the condition of the specimens at each stage of the campaign, providing the values of the dynamic modulus of elasticity. The ultrasonic pulses velocity tests were performed according to ASTM C597-16 [52], with direct and indirect configurations. The natural frequency of vibration was measured according to ASTM C215-19 [53], with longitudinal and transversal configurations. The different test layouts are shown in Fig. 4.

Four different indices were introduced, defined as the ratio between the pre-cracked/cured and the uncracked measure, allowing to trace the evolution of the damage-recovery process over time.

3.5. Sustained loading

In order to evaluate the effectiveness of the self-healing, a controlled damage was induced to the specimens by means of four-point bending tests, with 100 kN MTS machine at 0.15 mm/s displacement control. All the specimens were loaded up to 200 μm crack opening displacement (COD), measured at the tensile face with two LVDTs over a 150 mm distance across the mid span (i.e., maximum constant moment region); upon unloading the residual COD ranged between 50 and 100 μm. The targeted COD allowed to reach the strain-hardening multiple-cracking regime, and the damage resulted to be appropriate to analyse the self-healing capacity of the materials, as presented in Section 4. Furthermore, the cracks could be detected and clearly captured with the digital microscope.

The maximum load recorded during the pre-cracking process of each

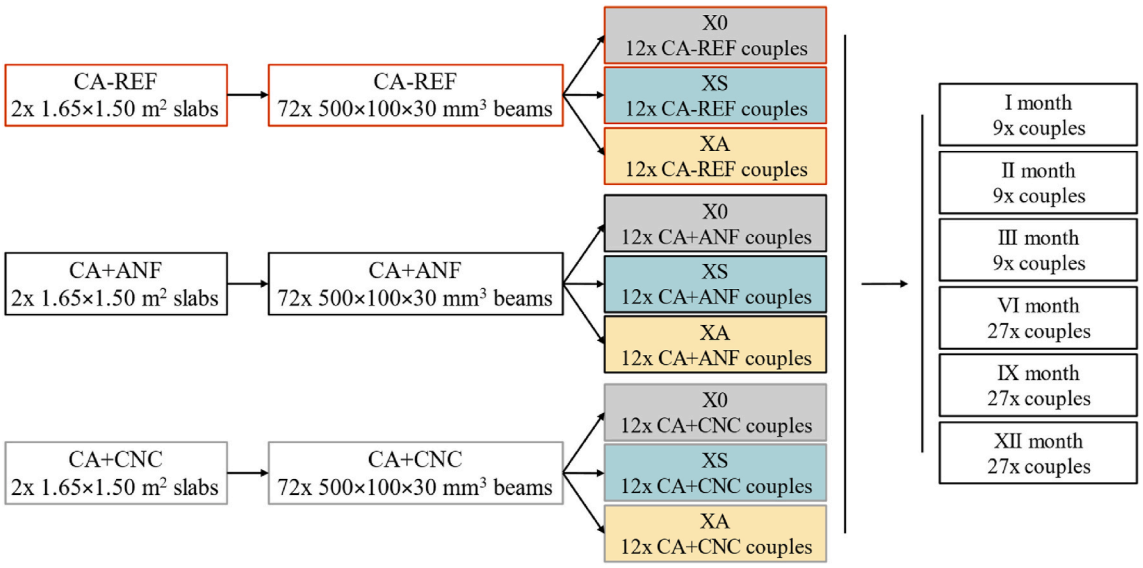

Fig. 1. Scheme of the specimens for the experimental campaign.

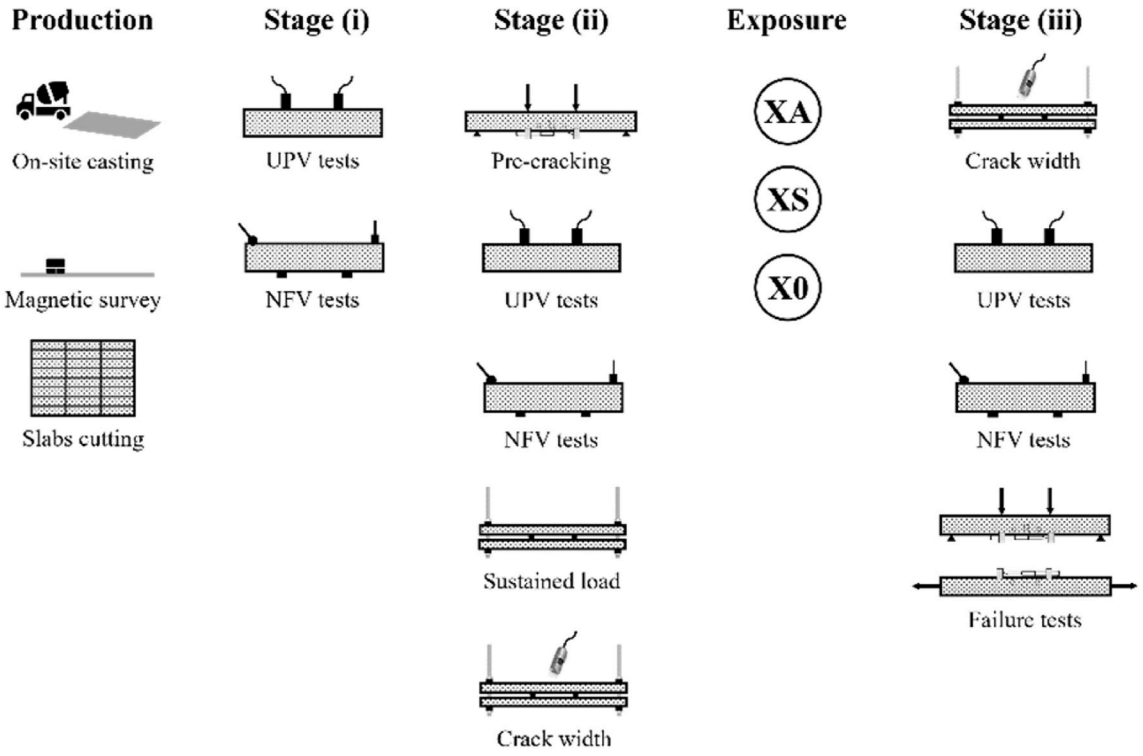

Fig. 2. Layout of the experimental campaign.

specimen was taken as the target value for the application of the sustained load during the period of exposure. The loading setup, shown in Fig. 5, is a stainless steel frame that braces two coupled specimens; therefore, a similar maximum load was assumed as coupling criterium. The frame is made of two cylinders placed between the specimens and four rectangular bars in the outer part. Four threaded rods allowed to apply the load onto the thin beams and keep them under the same position over time. The setup proposed reproduces a four-point bending flexural loading scheme, inducing a deformation to the beams by tightening the nuts, thus applying the load.

The load was transferred as follows (Fig. 6): (i) tightening the top nuts (red) to load the load cells; (ii) tightening the mid nuts (green) to transfer the load to the beams; (iii) releasing the top nuts and the load cells.

A preliminary evaluation of the capability of the bracing system to maintain a constant load applied to the coupled specimens over time was carried out, resulting in a limited loss, less than 10% of the applied initial load. Therefore, the observed loss was included in the force applied for the sustained load, to consider the prescribed loading regime as the lower threshold during the exposure time.

3.6. Cracks measurement

The crack width was measured at two different steps, before (stage ii)

(a) Scheme of the sensor (b) Grid layout

Fig. 3. Magnetic sensor for steel fibres survey (a) Scheme of the sensor (b) Grid layout.

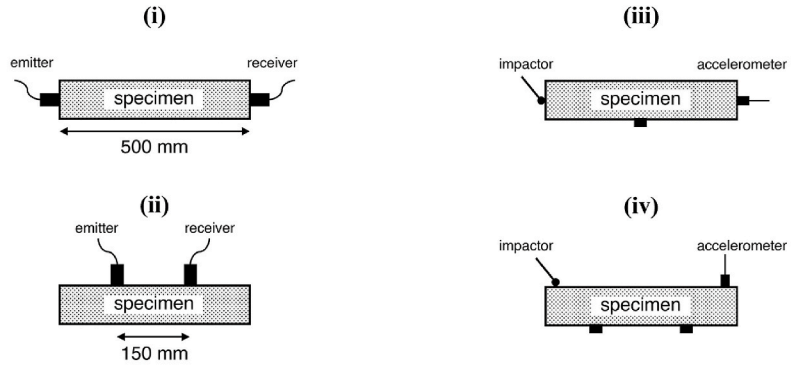

(a) UPV: direct (i), and indirect (ii) (b) NFV: longitudinal (iii), and transversal (iv)

Fig. 4. Non-destructive tests layout (a) UPV: direct (i), and indirect (ii) (b) NFV: longitudinal (iii), and transversal (iv).

and after (stage iii) the exposure, with the specimens inserted into the sustained load frame. Two different areas were defined dividing the mid span region into halves. Given the large number of specimens in the study, combined with the demand of time for image processing – only one crack per side was analysed, as shown in Fig. 7a. The criteria adopted for the selection of the cracks were verticality, width, and linearity. The total number of cracks was also determined scanning the cracked region horizontally (Fig. 7b); therefore, average crack width and spacing could be evaluated according to the measured COD.

A Dino-Lite portable digital microscope was used to take the images from the tensile surface of the beams. The frames taken were overlapped and merged with the software Photoshop, obtaining the complete profile of the crack, and the dimensions were converted from pixels to mm. Two different methods were used to create the binary image (i.e., an image where the profile of the crack is black and the other pixels are white, or vice versa); for the manual procedure, the single pixels of the crack were selected all along the profile, isolating them from the remaining parts of the merged picture. As an alternative, the deep learning software DeepCrack [54] was evaluated, comparing the results with cracks analysed manually, resulting in a limited error; 1% for the cracks at stage ii, and 6% at stage iii (Fig. 8). While for the former the deep learning code was considered reliable, for the latter, in light of the higher scattering of the results, the manual method was preferred.

3.7. Exposure of the specimens

After the crack width evaluation, the specimens, coupled into the sustained loading frame, were put inside containers, and exposed to the three different environments, respectively immersed in geothermal water, that was shipped from the power plant were the pilot structure is located, into a 3.3% NaCl solution to simulate the marine environments, both meant as aggressive scenarios, and in tap water, to be considered as a reference. In each container, specimens from the different materials went under exposure for up to one year.

3.8. Destructive tests

At the deadlines of one, two, three, six, nine and twelve months, six specimens per each mix and per each exposure condition were surveyed once again for crack width and non-destructive tests and finally tested up to failure to evaluate their mechanical recovery or deterioration (Fig. 9). From each couple of beams, one was tested under four-point bending up to failure to obtain the post-exposure flexural stress-COD curve and the stress-displacement response; the other specimen of the couple was tested under direct tension to extract the tensile constitutive law. The latter was then compared to the constitutive behaviour obtained through inverse analysis of the flexural tests [55]. The failure tests concluded the stage (iii) of the experimental campaign (Fig. 2).

4. Results

4.1. Cracks opening and sealing

Owing to the previously described properties of UHDC, the pre-cracking process resulted into the formation of multiple cracks within the mid span of the tensile face of the specimens, limiting the crack opening to 2–85 μm, as confirmed by the observations with the digital microscope. Similar crack width ranges were observed in Cuenca et al. [43], where the target total crack opening was 150 μm. The presence of nano-additives enhanced the willingness to form smaller cracks, as

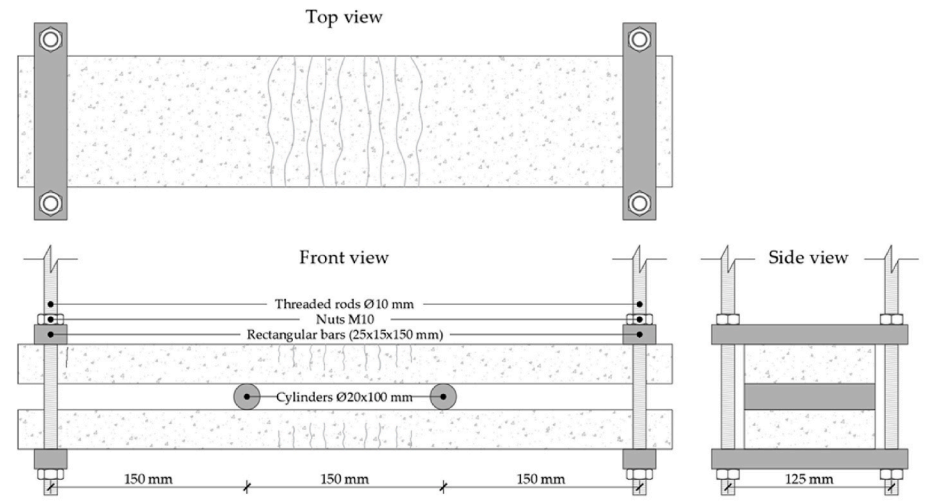

Fig. 5. (a) Layout of the sustained load frame, and (b) application of the sustained load.

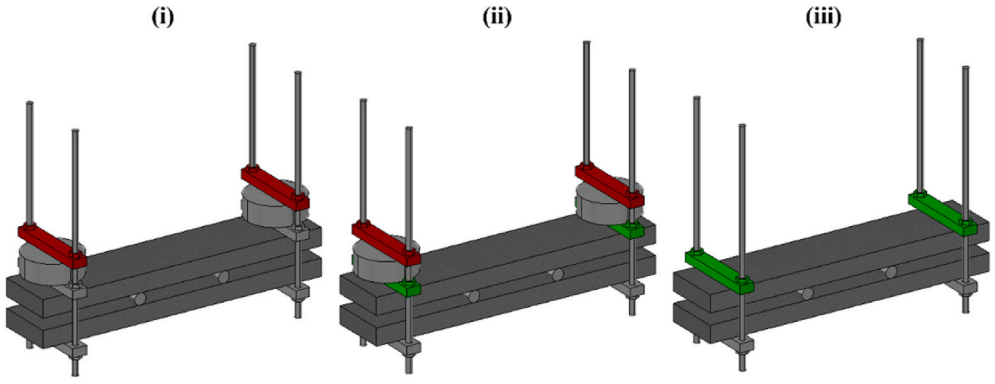

Fig. 6. Phases for the application of the sustained load.

reported in Fig. 10; most of the wider cracks happened in the reference mix, with a total amount of 11 for cracks of 30 μm or more, compared to the 7 in both alumina and cellulose mixes, while in the range 0–20 μm most of the cracks are referred to the latter.

Considering the crack width distribution, the mix with alumina nano-fibres tends to control the crack opening, promoting a better spreading of the damage instead of the localisation on a smaller number of cracks, due to the bridging effect provided by the alumina fibres at nano-scale level. An analogous contribution is offered by the cellulose nanocrystals, resulting in a similar distribution of crack widths.

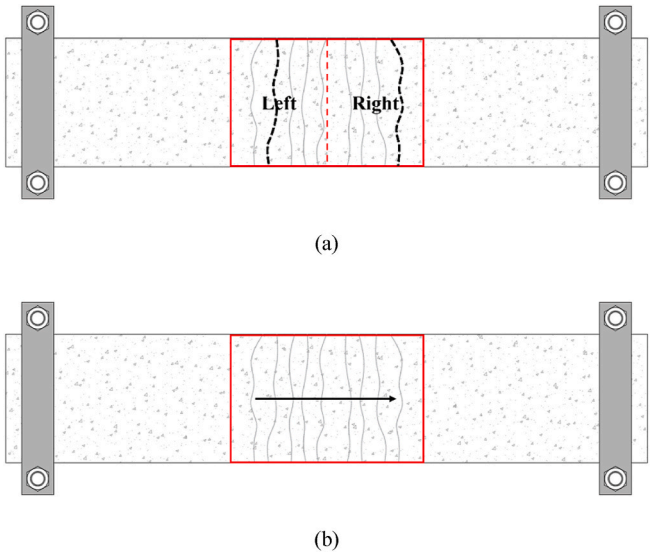

Fig. 7. (a) Single cracks from the two sides, and (b) horizontal scan of the mid span.

To evaluate the effectiveness of the healing/sealing, a specific index of crack sealing (ICS) was defined as the ratio between the healed area of the crack $A_{c,h}$ and its initial area $A_{c,0}$; the residual crack area was obtained as the difference between $A_{c,0}$ and the crack area measured after exposure $A_{c,1}$. The definition of the index is reported in Eq. (1).

$$ICS = \frac{A_{c,h}}{A_{c,0}} = \frac{A_{c,0} - A_{c,1}}{A_{c,0}} \quad (1)$$

The self-healing process activated immediately after the damage occurred, leading to a substantial reduction of the cracked area. After the first month of exposure, the ICS reached values of 0.90 for both cellulose and reference mixes (Fig. 11a), while the mix with nano-alumina was able to almost heal the damage completely since from the earliest exposure times. The influence of nano-additives became even more significant after the third month, when the recovery of the mix with alumina was still above the others, but the one with cellulose showed an increasing trend as well. The subsequent measures confirmed the pattern, with the two mixes with nano-additives approaching the complete recovery, while the reference lied slightly below. No open crack could be detected with the microscope after 9 months among all the specimens of the three mixes. The initial trend, up to 6 months of exposure, can be compared to the experimental results of Cuenca et al. [44]. In that case, the conditioning process inside geothermal water led to a recovery of approximately 80% after one month, with a progressive slight increase over time. Since the second month of exposure was not included, the comparison should be done with values at 1, 3, and 6 months, which are similar.

The aforementioned contribution of nano-additives actively affected the healing process, whose effectiveness was related to the dimensions of the cracks formed by the pre-cracking. The limitation on the crack width, due to the bridging effect provided by alumina nano-fibres and cellulose nanocrystals at nanoscale, facilitated the activation of the healing, while the minor volume could be sealed in a shorter period. Moreover, cellulose nanocrystals proved to facilitate the formation of C–S–H inside the voids of the matrix, owing to their high crystallinity index [56], thus contributing to fill the cracks since the earliest stages. Chloride exposure may have promoted the sealing process (Fig. 11b) owing to the chloride binding capacity of the matrix, as already observed by Cuenca et al. [43]; the precipitates formed cooperated to fill the voids. Conversely, for the specimens exposed to geothermal water, the sulphates inside the water likely altered the chemical process since they tend to react with calcium hydroxide; the controlled dimensions of the exposed area limited the availability of reagent, allowing the healing process to prevail over longer periods of exposure. The reference exposure in tap water, labelled as X0, is located between the two previously mentioned. On the one hand, tap water did not foster the sealing process as might have happened with chlorides; on the other, the negative contribution observed for geothermal water, rich in detrimental ions, did not affect the reference exposure. Moreover, in tap water the only chemical process that might actively counter the healing is the migration of Ca^{2+} ions – necessary for the healing process – from concrete matrix to water, whose duration is limited to the early stages.

Table 3 shows the composition of the three exposure waters after keeping the specimens inside for twelve months. Chloride content in the 3.3% NaCl solution decreased to 2%, agreeing with the hypothesis of chloride binding processes happening inside the UHPC matrix. The analyses confirmed the high content of sulphates for geothermal water. Moreover, the calcium content should be mainly related to the composition of the water itself, which can vary on a wide range (1.43–35,500 mg/kg) [57], since no leaching was observed on the surface of the specimens (Fig. 12). Only part of the calcium ions possibly leaked from the cracks formed.

A further observation (Fig. 7b) was implemented for some specimens to verify the actual multiple cracking regime both after pre-cracking and at failure under 4-point bending. Furthermore, the investigation allowed to determine the global healing framework in the constant moment

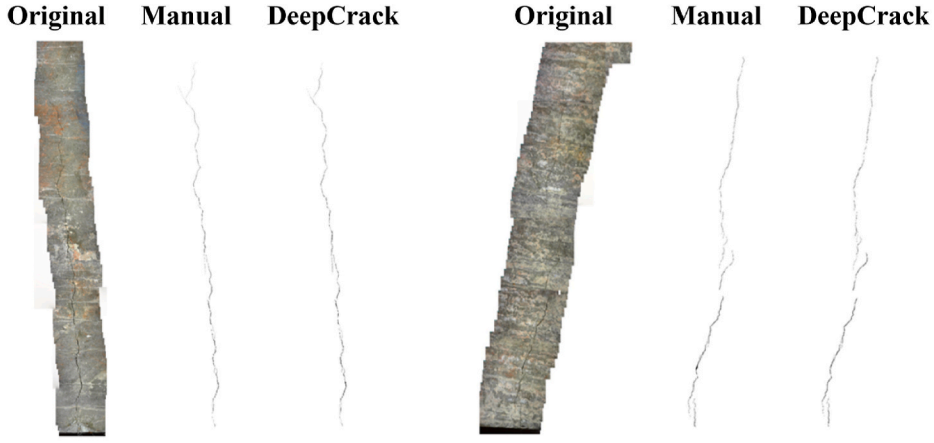

Fig. 8. Examples of crack area analysis and image processing (a) CA-REF, 1 month exposure (X0) (b) CA + CNC, 3 months exposure (XA).

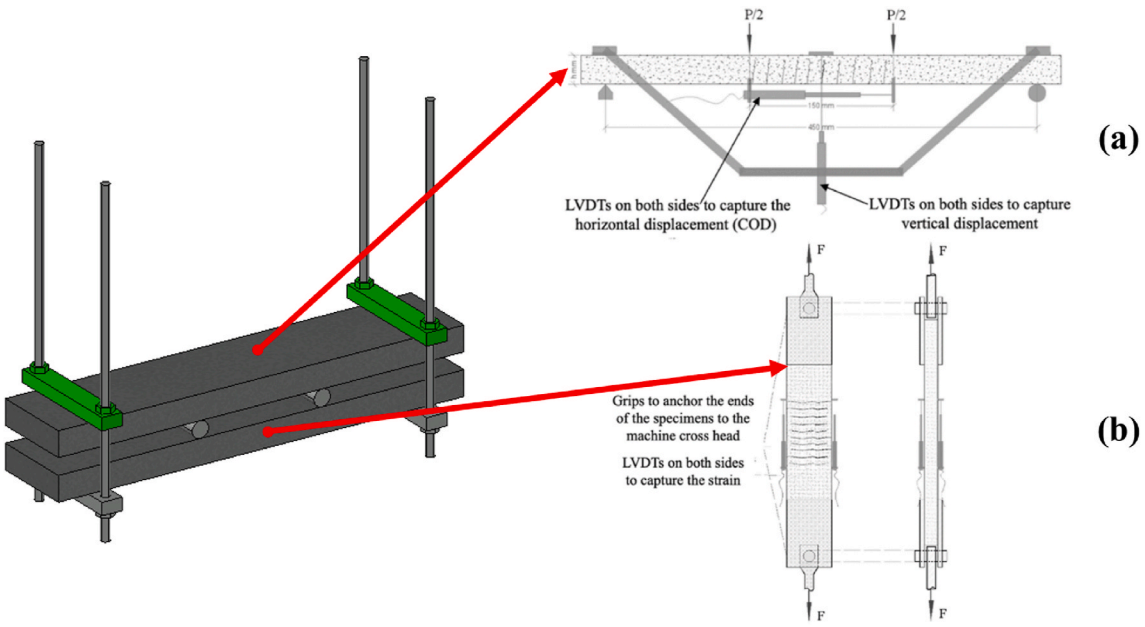

Fig. 9. Destructive tests layout; (a) 4-point bending, and (b) direct tension.

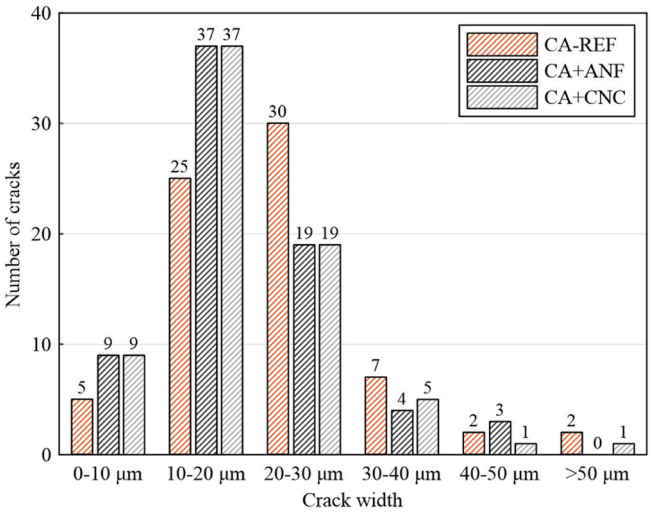

Fig. 10. Crack width distribution per material.

region, counting the healed cracks and comparing them to the initial condition.

Considering the pre-cracking stage, for all the cases considered at least four cracks were observed; specimens with cellulose nanocrystals exhibited a pronounced multiple cracking regime, with 10–12 cracks per specimen (Fig. 13). Only in two cases one and two cracks could not heal completely, respectively for the reference mix and for the one with cellulose nanocrystals, both exposed to geothermal water; the results substantiated the trend obtained from the index of crack sealing. The effectiveness of the healing/sealing process was confirmed during 4-point bending failure tests, where the load applied to the beam did not affect the previously formed cracks, rather resulting into the opening of new ones; in addition, all the materials were able to further develop the multiple cracking regime before the localisation on one single crack.

4.2. Evaluation of self-healing through non-destructive measurements

Together with the direct observations with digital microscope, non-destructive measurements allowed to indirectly estimate the reconstructed integrity of the beams after the periods of exposure. Fig. 14 shows the evolution of the healing ratios sorted by material with reference to the dynamic elastic modulus, measured by means of non-destructive tests, natural frequency of vibration (NFV) and ultrasonic pulses velocity (UPV) respectively. The indices are calculated as the ratio between the condition considered C_j – either after pre-cracking or after curing – and the original performance of the sound specimen C_0 (Eq. (2)). The damage induced with the pre-cracking process resulted in a reduction of the values of about 10%, with reference to the initial condition.

$$HR = \frac{C_j}{C_0} \tag{2}$$

Considering the natural frequency of vibration (Fig. 14a), the recovery registered after one month allowed to achieve performances close to the original condition, ranging between 96 and 99% of the original value. The healing process showed a further progress on the second month and was completed after three months for all the cases. The values observed after curing can be considered constant, since their variability is within the scattering of the different measures. The slight increase at 6 and 9 months is related to the stiffer response of the healed materials with respect to the virgin one, as better explained in the next section; this phenomenon is particularly remarkable for the reference mix.

For ultrasonic pulses (Fig. 14b) the recovery was already complete at the first month, and the response remained constant until 9 months, where a sudden increase of the values was registered; this variation can be related to the completion of the sealing process described in the previous section. No significant contribution from nano-additives could be observed; contrariwise, the reference mix showed a higher recovery, owing to the better properties of the sealing materials compared to the initial one. Furthermore, the non-destructive measurements address the bulk behaviour of the beam, which is not directly related to bridging effect at nanoscale, unlike other mechanical properties.

The three different environments did not affect the recovery process with reference to the non-destructive measurements, as shown in Fig. 15. The trend is comparable to what described for the materials, with a fast recovery, completed within three months for natural frequency and after one month for ultrasonic pulses, a constant response until the ninth month of curing, and a slight decrease at twelve months,

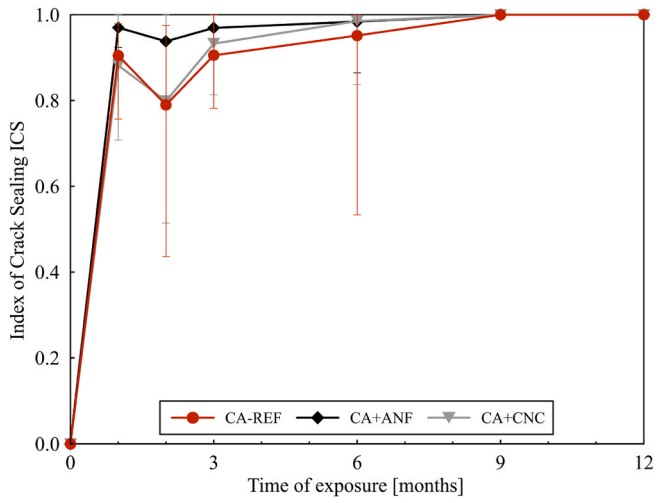

(a)

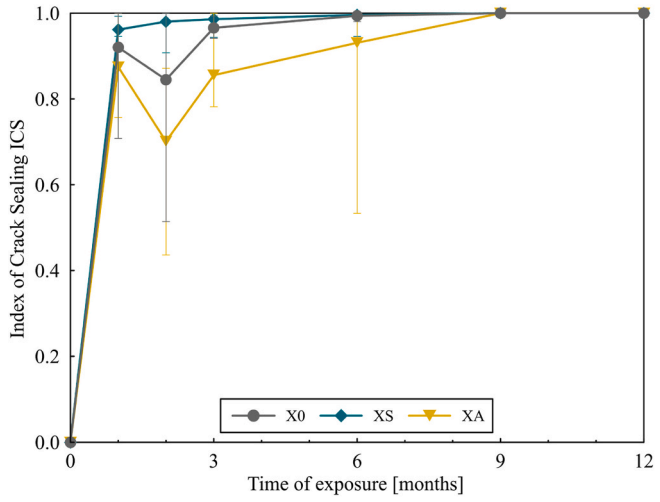

(b)

Fig. 11. Index of Crack Sealing (a) sorted by material, and (b) sorted by exposure.

Table 3
Chemical composition of the exposure water after 12 months.

Exposure	Chlorides	Sulphates	Mg	Ca	Fe
	[mg/l]	[mg/l]	[mg/l]	[mg/l]	[mg/l]
Tap water (X0)	50.7	64.4	8.0	3.0	3.8
3.3% NaCl solution (XS)	19,850	122.5	16.9	7.1	2.0
Geothermal water (XA)	41.0	5714	12.8	203.4	2.7

more pronounced for ultrasonic pulses. Between 9 and 12 months, no further healing was observed, since all the analysed cracks were already sealed; meanwhile, creep effect increased the permanent deflection of the beams, as clearly visible in Fig. 16. The progressive deformation of UHPC up to 12 months due to creep was already observed in Ref. [58].

For all the cases, the two different methods of measurement – transversal/indirect and longitudinal/direct – resulted in similar outputs in terms of healing ratio since the overall damage was localised into the central part of the beam and could be addressed by both types of measurements.

Fig. 12. Surface of a specimen exposed in geothermal water after twelve months.

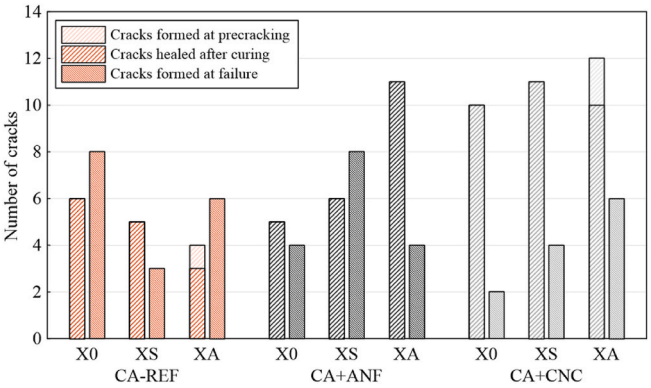

Fig. 13. Number of cracks formed and healed after three months.

4.3. Comparison of non-destructive methods

The different methodologies proposed to evaluate the condition of the material over time by means of non-destructive testing are herein compared. In both cases, two possible testing layouts were implemented to comply with possible limitations for on-site measurements.

The standards [52,53] provide the formulations to obtain a dynamic elastic modulus from either the natural frequency of vibration – depending on the excitation layout – or the velocity of ultrasonic waves. Fig. 17 shows the comparison among the four methods in terms of elastic modulus; the values displayed are referred to uncracked and pre-cracked stages. An additional column is provided with the experimental value measured by Cibelli [59] on the reference mix (CA-REF). In all cases the differences recorded are not significant, specifically for the two specimens with nano-additives. Moreover, the static modulus obtained through destructive test has a 2% difference if compared to the average of the dynamic values. On the other hand, both the mix with nano-alumina and nano-cellulose showed a slightly stiffer response in terms of dynamic elastic modulus. This confirms the contribution of nano-additives to the mechanical response, as further discussed in the following sections. The dynamic elastic modulus derived from resonant frequency is comparable to the values observed by Dehghanpour et al. [60], between the cases of UHPC with 1.3% and 2.0% steel fibres.

A more detailed comparison between direct and indirect ultrasonic pulse velocities is shown in Fig. 18. For uncracked specimens, direct longitudinal waves travelled at approximatively 4.6 km/s, similarly to what observed by Dehghanpour et al. [60]. Furthermore, the point cloud clearly displays the effect of induced damage, which reduced the direct velocity to 4.2–4.5 km/s, and the subsequent healing. As already stated, the precipitates, which filled the cracks, not only restored the integrity of the matrix, but also enhanced the stiffness of the material, leading to faster time of flight of the ultrasonic waves. Indirect longitudinal waves

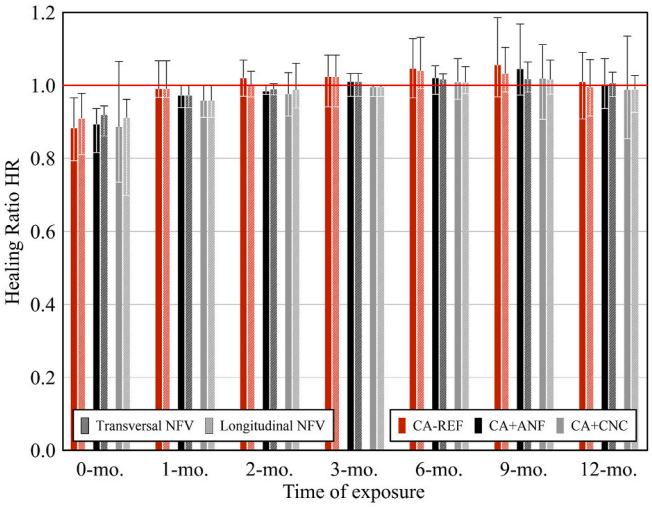

(a)

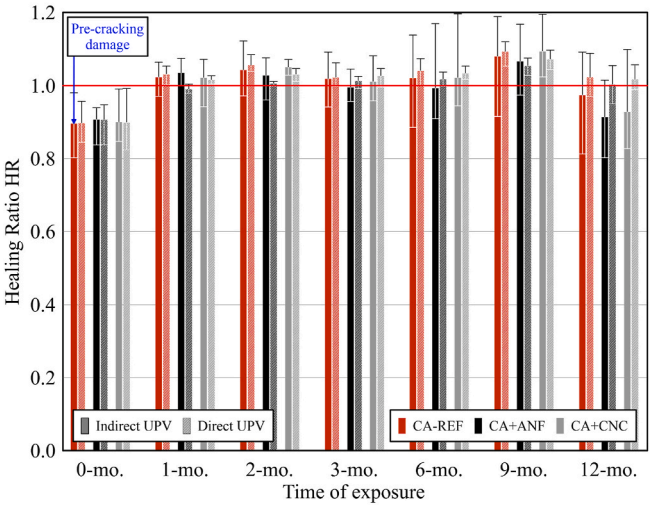

(b)

Fig. 14. Non-destructive measurements sorted by material; (a) Natural Frequency of Vibration, and (b) Ultrasonic Pulses Velocity.

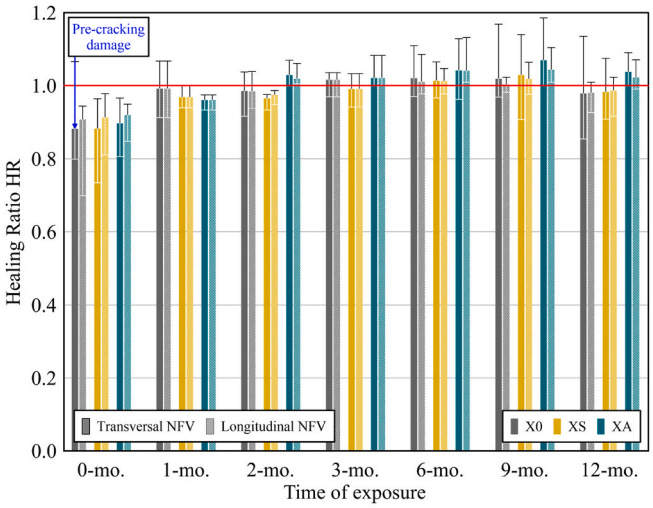

(a)

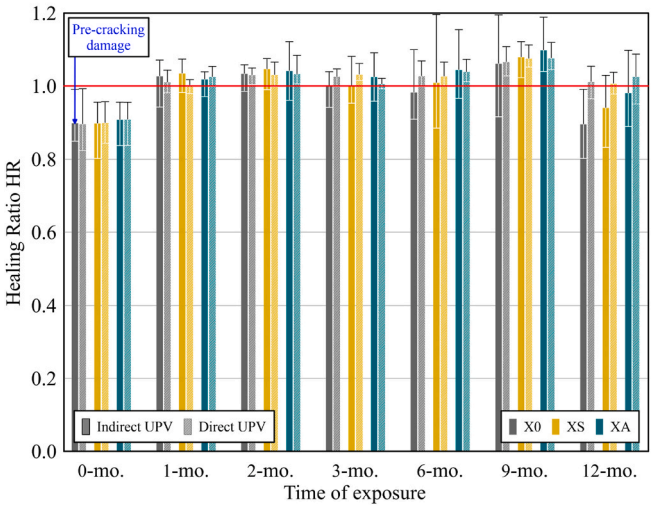

(b)

Fig. 15. Non-destructive measurements sorted by exposure; (a) Natural Frequency of Vibration, and (b) Ultrasonic Pulses Velocity.

experienced a more pronounced scattering. Moreover, in most cases, direct measurements achieved higher velocity than indirect waves. Both phenomena are related to the layout of the test; for direct UPV, the waves can easily follow the fastest path from the emitter to the receiver, with minor influence of eventual defects in the matrix. Conversely, indirect waves have a forced path in a limited span and are strongly affected by any factor such as heterogeneity of the matrix or fibres.

4.4. Stiffness and strength recovery

The Index of Stiffness Recovery defined in Eq. (3) was used to evaluate the stiffness recovery related to the flexural response at pre-cracking and at failure of each specimen after being in exposure for the scheduled period. The K parameters represent the stiffness of the specimen with reference to the Stress-COD curve; the subscripts *c,0* and *c,1* refer to the loading branch respectively at pre-cracking and after exposure, while the subscript *s,0* is related to the unloading stiffness after pre-cracking, as shown in Fig. 19.

$$ISR = \frac{K_{c,1} - K_{s,0}}{K_{c,0} - K_{s,0}} \quad (3)$$

The initial value of the index was determined from preliminary tests on intact beams, where the re-loading happened immediately after unloading. Fig. 20 shows how the healing process affected the mechanical response of the specimens, stiffening the initial response ($K_{c,1}$).

An early recovery was observed for all the materials, specifically for the mix with alumina nano-fibres, whose response was already comparable with the intact material after the first month; the index progressively increased over time. The alumina nano-fibres play a key role in bridging cracks at nanoscale, contributing with a remarkable mechanical resistance to the overall performance of the beam under flexural loads; if compared to the other mixes, the one with nano-alumina performed slightly better in most cases (i.e., 1, 3, 6, and 9 months), being similar to the others in the remaining periods. The mix with cellulose nanocrystals recovered completely after two months, the healing index settling around 1.0 for the subsequent periods; while the contribution of this specific nano-additive is remarkable in terms of crack bridging and healing promotion, from a mechanical point of view the effect is negligible, as compared to the reference mix. Considering the latter, the increase observed at 12 months can be related to the healing products formed inside the cracks, whose amount was directly proportional to the crack width. The scattering observed in Fig. 20b indicates how the

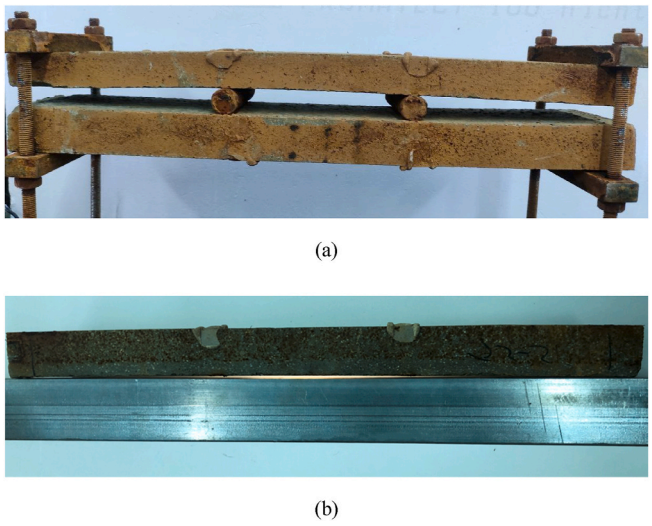

(a)

(b)

Fig. 16. Deflection of the beams after twelve months of exposure (a) under sustained loading, and (b) without applied load.

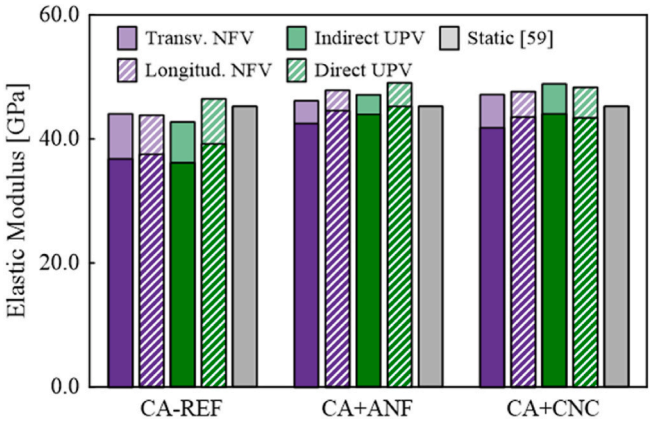

Fig. 17. Comparison among dynamic elastic modulus and experimental values from [59].

stiffness response is strictly related to the type of material analysed and not affected by the exposure. While the chloride solution led to variable results, for both tap water and geothermal water there was a linear increasing trend after 6 months, when the chemical processes delaying the healing (i.e., Ca^{2+} ions and sulphates for tap water and geothermal water respectively) can be considered concluded. A remarkable scattering was also observed in Ref. [44], which investigated the mix herein labelled as CA + ANF, and in Ref. [61], where the mix studied was CA + CNC. Lo Monte and Ferrara [20] achieved a stiffness recovery of 80% after one month of exposure for XA-CA mixture, the same value obtained for CA-REF in the present work. For longer periods, the re-cracking led to constant values of stiffness recovery, while Fig. 20a shows an increasing performance up to a complete recovery already after two months. As a matter of fact, the effect of sustained loading is less significant than repeated damage since the stable conditions of the specimens allow a steady recovery process.

The mechanical performance of the beams was also evaluated with respect to the peak stress reached during the 4-point bending failure tests after exposure. According to the results, shown in Fig. 21, the response of all the mixes remained approximately constant over time, proving the resilience of this type of material even under aggressive conditions. Fibres content and orientation are governing factors for the flexural behaviour of UHDC, leading to a wide range of results within the single beams. Conversely, the average values were not affected by the applied mechanical and environmental conditions and their variations were lower than the scattering among the single tests. A steady mechanical performance was already observed by Matos et al. [62], where the specimens underwent one year of chloride exposure with initial damage and sustained loading applied.

Similarly to what was observed in terms of stiffness, the mix with alumina nano-fibres generally performed better than the reference one owing to the mechanical characteristics of the nanoparticles and their crack bridging capability at nanoscale.

The evolution of stress-COD curves is another effective instrument to evaluate the mechanical performance over time, able to include the whole response instead of a single point. Fig. 22 confirms the results of the peak stresses, showing how the variability of the average curves is considerably lower than the scattering obtained within the tests, represented with the envelope (area filled).

The persistence of a strain hardening response in the flexural tests indicates the absence of degradation of the steel fibres embedded in the matrix, confirming the resistance to corrosion of UHPC fibre reinforcement [19]; although the exterior layers showed visible corrosion (Fig. 23a), the degradation did not penetrate inside the beams (Fig. 23b).

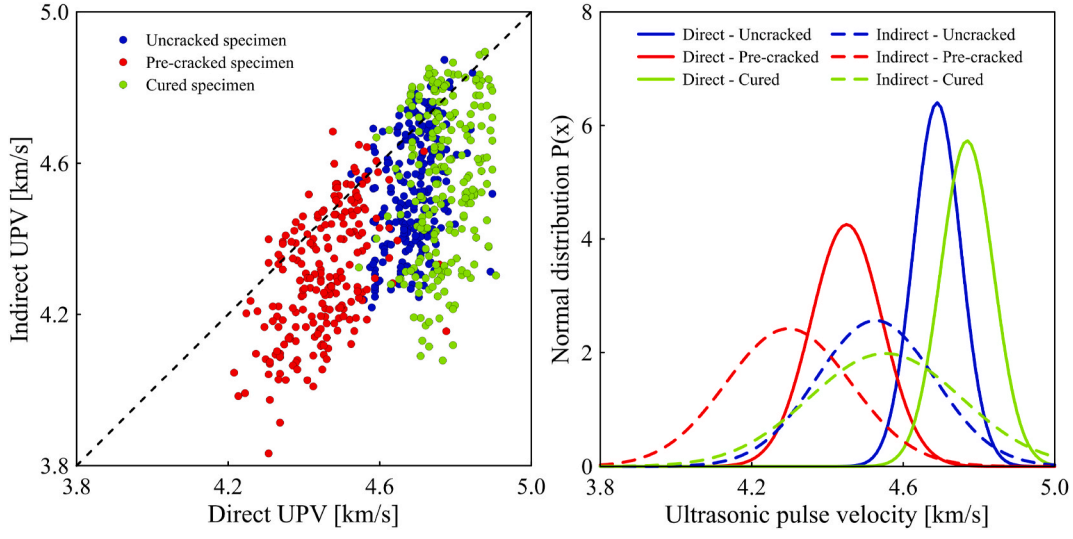

Fig. 18. Comparison between direct and indirect UPV values and normal distributions.

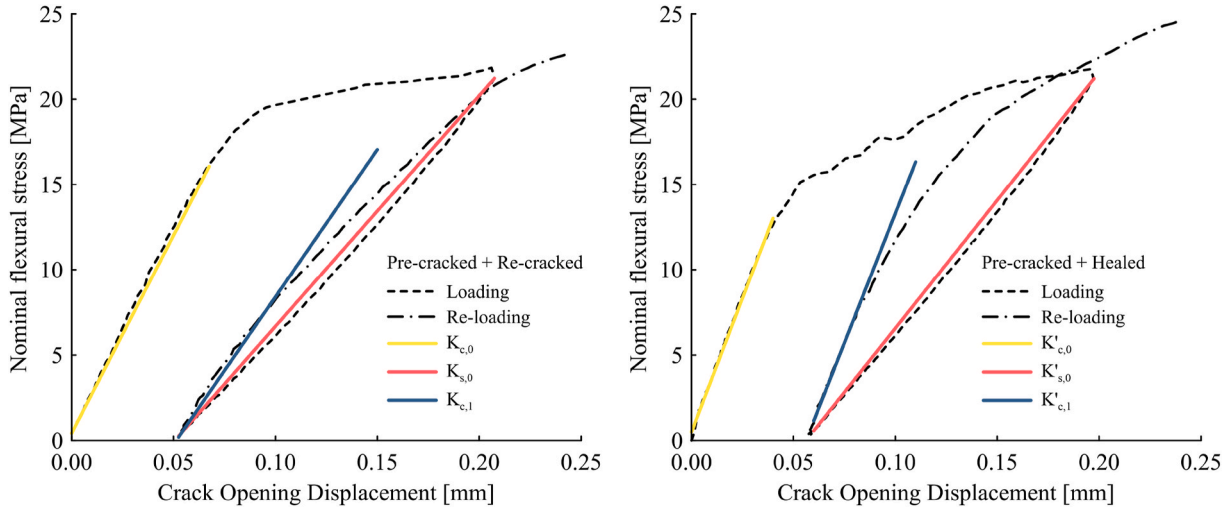

Fig. 19. Definition of the Index of Stiffness Recovery with and without curing.

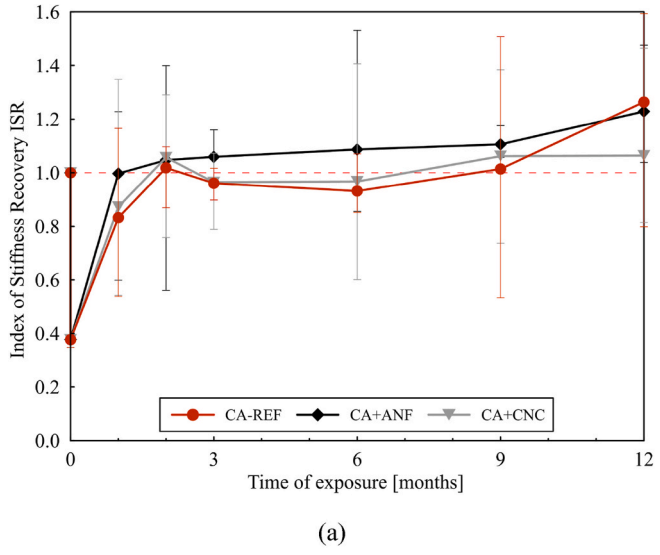

Fig. 20. Index of Stiffness Recovery (a) sorted by material, and (b) sorted by exposure.

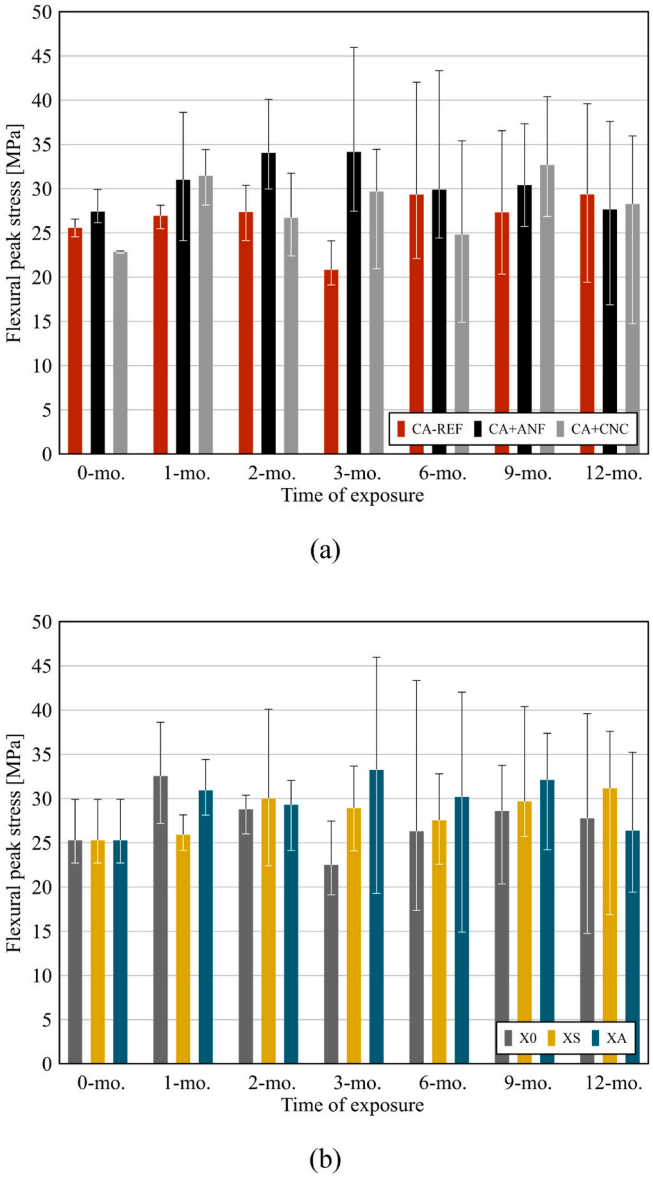

Fig. 21. Flexural peak stress; (a) sorted by material, and (b) sorted by exposure.

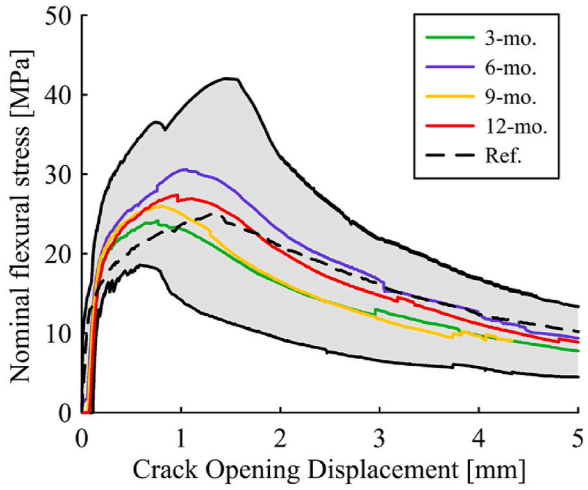

(a)

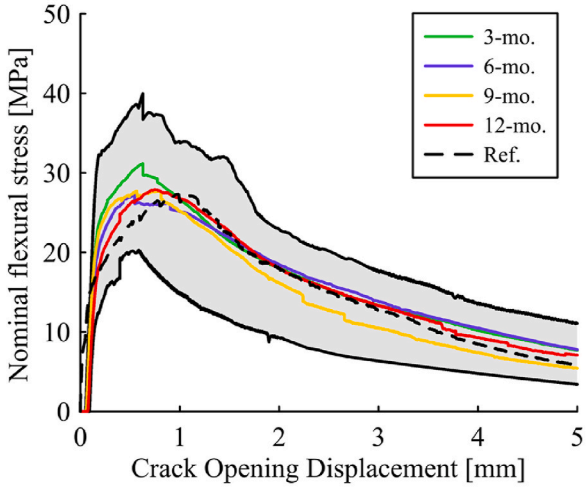

(b)

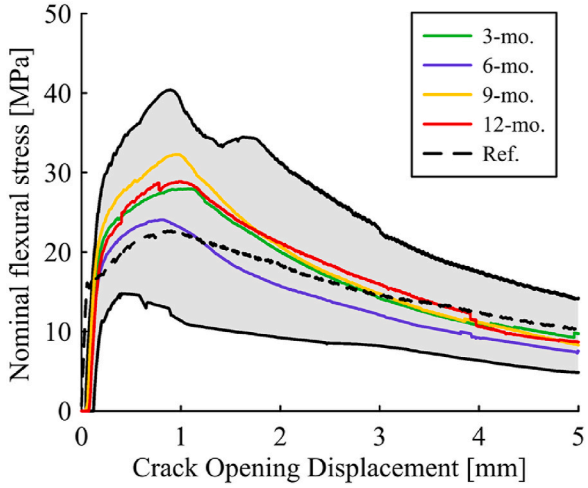

(c)

Fig. 22. Average stress-COD curves, sorted by material; (a) CA-REF, (b) CA + ANF, and (c) CA + CNC.

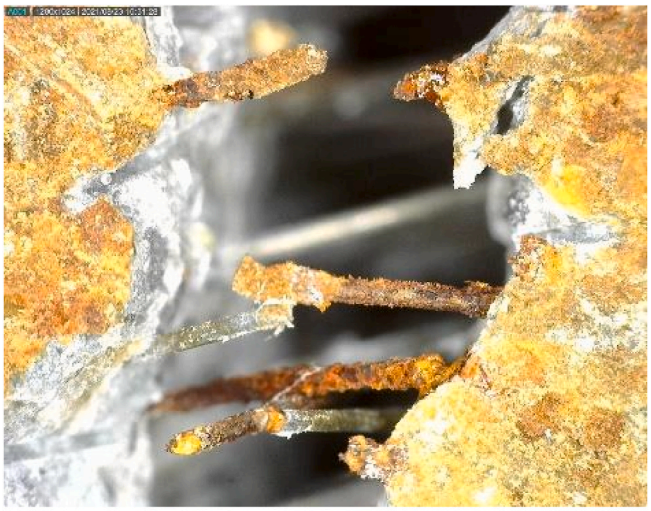

(a)

(b)

Fig. 23. Fibres condition after twelve months of exposure; (a) outer layer, and (b) inner layer.

5. Conclusions

The work herein presented investigated the effects of mechanical and environmental loads simultaneously applied to Ultra-High Durability Concrete (UHDC) specimens, considering the influence of autogenous healing over time promoted by a crystalline admixture in a synergic effect with nano-constituents (alumina nano-fibres and cellulose nano-crystals) as a further mean to control the crack opening. Besides a reference exposure condition, consisting in continuous tap water immersion, continuous immersion in a 3.3% NaCl solution and in a geothermal water obtained from a geothermal power plant were investigated as representatives of extremely aggressive scenarios for which UHDC could represent the ideal material solution for structural applications demanding high durability. A dedicated experimental methodology was proposed and validated, including both non-destructive and destructive measures, including a tailored set-up for the sustained flexural load application, which allowed to assess the evolution of the mechanical performance in the aforesaid intended scenarios together with the measurement of cracks sealing through direct observations with digital microscope. Different indices were

introduced to characterize the healing effectiveness over different periods of time, defining the recovery with respect to the intact and damaged conditions.

Based on the methodology presented in this study along with the obtained results, the following conclusions can be drawn.

- The healing mechanism activated from the beginning of the exposure period, compensating the induced damage already within three months; the healing/sealing process was not affected by sustained loads applied to the beams, even considering that a constant deflection actively kept the cracks opened during the curing periods.
- The observations with digital microscope provided direct and reliable measurements of the physical conditions of the material, necessary to correlate the chemical processes with the mechanical response obtained from the other tests. Most of the formed cracks had a limited width, owing to the peculiar properties of UHDC; this contributed to foster the healing/sealing process and to close the cracks at early stages.
- The indices proposed in the study proved to be effective to evaluate the evolution of the performance of UHDC over time, being in good agreement among each other and with the parameters from mechanical tests.
- All the three mixes showed a comparable behaviour both in terms of crack sealing capacity and mechanical response. Alumina nanofibres enhanced the performance of the reference material effectively bridging the cracks at nanoscale, limiting the crack width, and promoting an easier and earlier effective healing process. Cellulose nanocrystal provided a similar contribution to guarantee a smeared crack pattern but did not affect the mechanical response.
- The mechanical performance of the material remained constant over the different periods, and comparable to the reference tests without pre-cracking; owing to UHPC material properties, corrosion phenomena did not penetrate inside the matrix and only involved the very exterior surface of the specimens, ensuring the upkeep of the flexural load bearing capacity of the beams. Moreover, the specimens exposed to geothermal water did not exhibit any leaching on the surface. The lower performances observed might be related to leaching occurring inside the cracks.
- Environmental conditions played a significant role in the first periods of exposure, up to 6 months, when the chemical interactions limited, in the case of geothermal water, or synergically acted with, in the case of chloride solution, the healing process; after longer periods, the differences among the three exposures were progressively reduced.
- Some observations showed variable trend at twelve months of exposure, suggesting that further monitoring might be helpful to better understand the ongoing phenomena at longer periods.

The proposed methodology proved how UHDC is a promising solution for a new design approach tackling both mechanical and durability requirements with a tailored solution, proving its capacity to preserve the mechanical performance, specifically in terms of tensile/flexural resistance, owing to its self-healing capability.

Declaration of competing interest

The authors declare that they have no known competing financial interests or personal relationships that could have appeared to influence the work reported in this paper.

Data availability

Data will be made available on request.

Acknowledgements

The research activity reported has been performed in the framework of the ReSHEALience project (Rethinking coastal defense and Green-energy Service infrastructures through enHancEd-durAbiLity high-performance cement-based materials) which has received funding from the European Union's Horizon 2020 research and innovation program under grant agreement No 760824. The information and views set out in this publication do not necessarily reflect the official opinion of the European Commission.

The logistic and technical support of LPM (Laboratory of Material and Structural Testing) at Politecnico di Milano is acknowledged, and in particular Antonio Cocco, Paolo Broglia, Giuseppe Pappadà and Marco Cucchi who actively helped in preparing and providing test setups and testing machines.

References

[1] B. Martin-Pérez, H. Zibara, R.D. Hooton, M.D.A. Thomas, A study of the effect of chloride binding on service life predictions, Cement Concr. Res. 30 (2000) 1215–1223.
[2] J. Gao, Z. Yu, L. Song, T. Wang, S. Wei, Durability of concrete exposed to sulfate attack under flexural loading and drying-wetting cycles, Construct. Build. Mater. 39 (2013) 33–38, https://doi.org/10.1016/j.conbuildmat.2012.05.033.
[3] Y. Dong, Performance assessment and design of ultra-high performance concrete (UHPC) structures incorporating life-cycle cost and environmental impacts, Construct. Build. Mater. 167 (2018) 414–425, https://doi.org/10.1016/j.conbuildmat.2018.02.037.
[4] D.Q. Nguyen, C. Brammer, M. Bagajewicz, New tool for the evaluation of the scheduling of preventive maintenance for chemical process plants, Ind. Eng. Chem. Res. 47 (2008) 1910–1924, https://doi.org/10.1021/ie071231i.
[5] S. Abbas, M.L. Nehdi, M.A. Saleem, Ultra-high performance concrete: mechanical performance, durability, sustainability and implementation challenges, Int J Concr Struct Mater 10 (2016) 271–295, https://doi.org/10.1007/s40069-016-0157-4.
[6] M. Shafieifar, M. Farzad, A. Azizinamini, Experimental and numerical study on mechanical properties of ultra high performance concrete (UHPC), Construct. Build. Mater. 156 (2017) 402–411, https://doi.org/10.1016/j.conbuildmat.2017.08.170.
[7] L. Ferrara, E. Cuenca, F. Lo Monte, D. Snoeck, N. De Belie, An application oriented state-of-art and research-need perspective on self-healing fibre-reinforced cementitious composites, in: Proceedings of the ACI-Fib-RILEM International Workshop, 2018, pp. 80–89. FRC2018.
[8] B.A. Graybeal, Compressive behavior of ultra-high-performance fiber-reinforced concrete, ACI Mater. J. 104 (2007) 146–152.
[9] S. Sritharan, Design of UHPC structural members: lessons learned and ASTM test requirements, Adv Civ Eng Mater 4 (2015) 113–131, https://doi.org/10.1520/ACEM20140042.
[10] C. Magureanu, I. Sosa, C. Negrutiu, B. Heghes, Mechanical properties and durability of ultra-high-performance concrete, ACI Mater. J. 109 (2012) 177–184.
[11] S. Al-Obaidi, P. Bamonte, F. Animato, F. Lo Monte, I. Mazzantini, M. Luchini, S. Scalari, L. Ferrara, Innovative design concept of cooling water tanks/basins in geothermal power plants using Ultra-High-Performance Fiber-Reinforced Concrete with enhanced durability, Sustainability 13 (2021) 1–26, https://doi.org/10.3390/su13179826.
[12] F. Lo Monte, L. Ferrara, Tensile behaviour identification in Ultra-High Performance Fibre Reinforced Cementitious Composites: indirect tension tests and back analysis of flexural test results, Materials and Structures/Materiaux et Constructions 53 (2020) 1–12, https://doi.org/10.1617/s11527-020-01576-8.
[13] Z. Zhou, P. Qiao, Direct tension test for characterization of tensile behavior of Ultra-High Performance Concrete, J. Test. Eval. 48 (2018), https://doi.org/10.1520/JTE20170644.
[14] Z. Li, H. Zhang, R. Wang, Influence of steel fiber distribution on splitting damage and transport properties of ultra-high performance concrete, Cem. Concr. Compos. 126 (2022) 1–15, https://doi.org/10.1016/j.cemconcomp.2021.104373.
[15] B.A. Graybeal, Tensile mechanical response of ultra-high-performance concrete, Adv Civ Eng Mater 4 (2015) 62–74, https://doi.org/10.1520/ACEM20140029.
[16] S. Zhao, L. Jiang, H. Chu, A preliminary investigation of energy consumption in fracture of ultra-high performance concrete, Construct. Build. Mater. 237 (2020) 1–12, https://doi.org/10.1016/j.conbuildmat.2019.117634.
[17] F. Bencardino, L. Rizzuti, G. Spadea, R.N. Swamy, Experimental evaluation of fiber reinforced concrete fracture properties, Compos. B Eng. 41 (2010) 17–24, https://doi.org/10.1016/j.compositesb.2009.09.002.
[18] F. Altmann, V. Mechtcherine, Durability design strategies for new cementitious materials, Cement Concr. Res. 54 (2013) 114–125, https://doi.org/10.1016/j.cemconres.2013.08.008.
[19] S. Wang, X. Guo, Z. Guo, C. He, X. Duan, W. Hu, K. Zhuang, Direct characterization of steel fibre corrosion in pre-cracked ultra-high performance concrete (UHPC) with different crack widths, Construct. Build. Mater. 315 (2022) 1–10, https://doi.org/10.1016/j.conbuildmat.2021.125769.
[20] F. Lo Monte, L. Ferrara, Self-healing characterization of UHPFRCC with crystalline admixture: experimental assessment via multi-test/multi-parameter approach,

Construct. Build. Mater. 283 (2021) 1–12, https://doi.org/10.1016/j.conbuildmat.2021.122579.
[21] M. Schmidt, S. Fröhlich, UHPC from research to standardization: European approaches, Adv Civ Eng Mater 4 (2015) 144–170, https://doi.org/10.1520/ACEM20140032.
[22] R.D. Hooton, Future directions for design, specification, testing, and construction of durable concrete structures, Cement Concr. Res. 124 (2019) 1–17, https://doi.org/10.1016/j.cemconres.2019.105827.
[23] R. Muigai, P. Moyo, M. Alexander, Durability design of reinforced concrete structures: a comparison of the use of durability indexes in the deemed-to-satisfy approach and the full-probabilistic approach, Materials and Structures/Materiaux et Constructions 45 (2012) 1233–1244, https://doi.org/10.1617/s11527-012-9829-y.
[24] S. Al-Obaidi, P. Bamonte, L. Ferrara, M. Luchini, I. Mazzantini, Durability-based design of structures made with ultra-high-performance/ultra-high-durability concrete in extremely aggressive scenarios: application to a geothermal water basin case study, Infrastructure 5 (2020) 1–44, https://doi.org/10.3390/infrastructures5110102.
[25] J. Li, Z. Wu, C. Shi, Q. Yuan, Z. Zhang, Durability of ultra-high performance concrete – a review, Construct. Build. Mater. 255 (2020) 1–13, https://doi.org/10.1016/j.conbuildmat.2020.119296.
[26] B.A. Graybeal, Simultaneous Structural and Environmental Loading of an Ultra-high Performance Concrete Component, Hachette, 2010.
[27] E.G. Moffatt, M.D.A. Thomas, A. Fahim, R.D. Moser, Performance of Ultra-High-Performance Concrete in harsh marine environment for 21 years, ACI Mater. J. 117 (2020) 105–112, https://doi.org/10.14359/51727022.
[28] Y. Yang, M.D. Lepech, E.H. Yang, V.C. Li, Autogenous healing of engineered cementitious composites under wet-dry cycles, Cement Concr. Res. 39 (2009) 382–390, https://doi.org/10.1016/j.cemconres.2009.01.013.
[29] L.-L. Kan, H.-S. Shi, A.R. Sakulich, V.C. Li, Self-healing characterization of engineered cementitious composite materials, ACI Mater. J. 107 (2010) 617–624.
[30] G. Yildirim, A. Alyousif, M. Sahmaran, M. Lachemi, Assessing the self-healing capability of cementitious composites under increasing sustained loading, Adv. Cement Res. 27 (2015) 581–592, https://doi.org/10.1680/adcr.14.00111.
[31] M. Li, V.C. Li, Cracking and healing of engineered cementitious composites under chloride environment, ACI Mater. J. 108 (2011) 333–340.
[32] D.J. Kim, S.H. Kang, T.H. Ahn, Mechanical characterization of high-performance steel-fiber reinforced cement composites with self-healing effect, Materials 7 (2014) 508–526, https://doi.org/10.3390/ma7010508.
[33] A. Negrini, M. Roig-Flores, E.J. Mezquida-Alcaraz, L. Ferrara, P. Serna, Effect of crack pattern on the self-healing capability in traditional, HPC and UHPFRC concretes measured by water and chloride permeability, in: MATEC Web of Conferences, EDP Sciences, 2019, https://doi.org/10.1051/matecconf/201928901006.
[34] V.Y. Garas, L.F. Kahn, K.E. Kurtis, Short-term tensile creep and shrinkage of ultra-high performance concrete, Cem. Concr. Compos. 31 (2009) 147–152, https://doi.org/10.1016/j.cemconcomp.2009.01.002.
[35] J.Y. Guo, J.Y. Wang, K. Wu, Effects of self-healing on tensile behavior and air permeability of high strain hardening UHPC, Construct. Build. Mater. 204 (2019) 342–356, https://doi.org/10.1016/j.conbuildmat.2019.01.193.
[36] A. Beglarigale, D. Eyice, B. Tutkun, H. Yazıcı, Evaluation of enhanced autogenous self-healing ability of UHPC mixtures, Construct. Build. Mater. 280 (2021) 1–16, https://doi.org/10.1016/j.conbuildmat.2021.122524.
[37] E. Özbay, M. Şahmaran, H.E. Yücel, T.K. Erdem, M. Lachemi, V.C. Li, Effect of sustained flexural loading on self-healing of engineered cementitious composites, J. Adv. Concr. Technol. 11 (2013) 167–179, https://doi.org/10.3151/jact.11.167.
[38] E. Parant, R. Pierre, F. Le Maou, Durability of a multiscale fibre reinforced cement composite in aggressive environment under service load, Cement Concr. Res. 37 (2007) 1106–1114, https://doi.org/10.1016/j.cemconres.2006.02.021.
[39] C. Desmettre, J.P. Charron, Water permeability of reinforced concrete with and without fiber subjected to static and constant tensile loading, Cement Concr. Res. 42 (2012) 945–952, https://doi.org/10.1016/j.cemconres.2012.03.014.
[40] Z. Ma, T. Zhao, X. Yao, Influence of applied loads on the permeability behavior of ultra high performance concrete with steel fibers, J. Adv. Concr. Technol. 14 (2016) 770–781, https://doi.org/10.3151/jact.14.770.
[41] J.P. Charron, E. Denarié, E. Brühwiler, Permeability of ultra high performance fiber reinforced concretes (UHPFRC) under high stresses, Materials and Structures/Materiaux et Constructions 40 (2007) 269–277, https://doi.org/10.1617/s11527-006-9105-0.
[42] P. Serna, F. Lo Monte, E.J. Mezquida-Alcaraz, E. Cuenca, V. Mechtcherine, M. Reichardt, A. Peled, O. Regev, R.P. Borg, A. Tretjakov, D. Lizunov, K. Sobolev, S. Sideri, K. Nelson, E.M. Gastaldo Brac, L. Ferrara, Upgrading the Concept of UHPFRC for High Durability in the Cracked State: the Concept of Ultra High Durability Concrete (UHDC) in the Approach of the H2020 Project ReSHEALience, 2019. Dennis Lizunov.
[43] E. Cuenca, F. Lo Monte, M. Moro, A. Schiona, L. Ferrara, Effects of autogenous and stimulated self-healing on durability and mechanical performance of UHPFRC: validation of tailored test method through multi-performance healing-induced recovery indices, Sustainability (2021) 13, https://doi.org/10.3390/su132011386.
[44] E. Cuenca, L. D'Ambrosio, D. Lizunov, A. Tretjakov, O. Volobujeva, L. Ferrara, Mechanical properties and self-healing capacity of ultra high performance fibre reinforced concrete with alumina nano-fibres: tailoring ultra high durability concrete for aggressive exposure scenarios, Cem. Concr. Compos. 118 (2021) 1–17, https://doi.org/10.1016/j.cemconcomp.2021.103956.
[45] E. Cuenca, M. Criado, M. Giménez, M.C. Alonso, L. Ferrara, Effects of alumina nanofibers and cellulose nanocrystals on durability and self-healing capacity of ultrahigh-performance fiber-reinforced concretes, J. Mater. Civ. Eng. 34 (2022) 1–17, https://doi.org/10.1061/(asce)mt.1943-5533.0004375.
[46] S. Al-Obaidi, M. Davolio, F.L. Monte, F. Costanzi, M. Luchini, P. Bamonte, L. Ferrara, Structural validation of geothermal water basins constructed with durability enhanced ultra high performance fiber reinforced concrete (Ultra High Durability Concrete), Case Stud. Constr. Mater. 17 (2022), https://doi.org/10.1016/j.cscm.2022.e01202.
[47] M.M. Islam, Q. Zhang, Q. Jin, A review of existing codes and standards on design factors for UHPC placement and fiber orientation, Construct. Build. Mater. 345 (2022) 1–17, https://doi.org/10.1016/j.conbuildmat.2022.128308.
[48] L. Ferrara, N. Ozyurt, M. Di Prisco, High mechanical performance of fibre reinforced cementitious composites: the role of "casting-flow induced" fibre orientation, Materials and Structures/Materiaux et Constructions 44 (2011) 109–128, https://doi.org/10.1617/s11527-010-9613-9.
[49] L. Ferrara, M. Faifer, S. Toscani, A magnetic method for non destructive monitoring of fiber dispersion and orientation in steel fiber reinforced cementitious composites-part 1: method calibration, Materials and Structures/Materiaux et Constructions 45 (2012) 575–589, https://doi.org/10.1617/s11527-011-9793-y.
[50] L. Ferrara, M. Faifer, M. Muhaxheri, S. Toscani, A magnetic method for non destructive monitoring of fiber dispersion and orientation in steel fiber reinforced cementitious composites-part 2: correlation to tensile fracture toughness, Materials and Structures/Materiaux et Constructions 45 (2012) 591–598, https://doi.org/10.1617/s11527-011-9794-x.
[51] T. Lei, R. Ottoboni, M. Faifer, S. Toscani, L. Ferrara, A cost-effective method to assess the fiber content and orientation in steel fiber reinforced concrete, in: 2019 IEEE International Instrumentation and Measurement Technology Conference (I2MTC), 2019.
[52] ACI International, ASTM C597-16: Standard Test Method for Pulse Velocity through Concrete, 2016, https://doi.org/10.1520/C0597-16.
[53] ACI International, ASTM C215-19: Standard Test Method for Fundamental Transverse, Longitudinal, and Torsional Resonant Frequencies of Concrete Specimens, 2020, https://doi.org/10.1520/C0215-19.
[54] Y. Liu, J. Yao, X. Lu, R. Xie, L. Li, DeepCrack: a deep hierarchical feature learning architecture for crack segmentation, Neurocomputing 338 (2019) 139–153, https://doi.org/10.1016/j.neucom.2019.01.036.
[55] S. Al-Obaidi, M. Davolio, G. Recchia, F. Lo Monte, L. Ferrara, How does self-healing under sustained loadings in aggressive water affect the constitutive response of a UHPFRC?, in: SHCC 2022, RILEM Bookseries, vol. 39, 2023.
[56] E.G. Deze, E. Cuenca, A.M.L. Násner, M. Iakovlev, S. Sideri, A. Sapalidis, R.P. Borg, L. Ferrara, Nanocellulose enriched mortars: evaluation of nanocellulose properties affecting microstructure, strength and development of mixing protocols, in: Mater Today Proc, Elsevier Ltd, 2021, pp. 50–56, https://doi.org/10.1016/j.matpr.2021.09.511.
[57] I. Dincer, M.F. Ezzat, Geothermal energy production, in: Comprehensive Energy Systems, Elsevier Inc., 2018, pp. 252–303, https://doi.org/10.1016/B978-0-12-809597-3.00313-8.
[58] V.Y. Garas, K.E. Kurtis, L.F. Kahn, Creep of UHPC in tension and compression: effect of thermal treatment, Cem. Concr. Compos. 34 (2012) 493–502, https://doi.org/10.1016/j.cemconcomp.2011.12.002.
[59] A. Cibelli, Computational Modelling of Ageing, Healing and Degradation of Ordinary and Ultra High Performance Concrete, Politecnico di Milano, 2022.
[60] H. Dehghanpour, S. Subasi, S. Guntepe, M. Emiroglu, M. Marasli, Investigation of fracture mechanics, physical and dynamic properties of UHPCs containing PVA, glass and steel fibers, Construct. Build. Mater. 328 (2022), https://doi.org/10.1016/j.conbuildmat.2022.127079.
[61] E. Cuenca, V. Postolachi, L. Ferrara, Cellulose nanofibers to improve the mechanical and durability performance of self-healing Ultra-High Performance Concretes exposed to aggressive waters, Construct. Build. Mater. 374 (2023), 130785, https://doi.org/10.1016/j.conbuildmat.2023.130785.
[62] A.M. Matos, S. Chaves Figueiredo, S. Nunes, E. Schlangen, J.L. Barroso-Aguiar, Durability of an UHPFRC under mechanical and chloride loads, Construct. Build. Mater. 311 (2021), https://doi.org/10.1016/j.conbuildmat.2021.125223.